Influence of wet-dry cycles on vertical cutoff walls made of reactive magnesia-slag-bentonite-soil mixtures

Hao-Liang Wu

Jiangsu Key Laboratory of Urban Underground Engineering & Environmental Safety, Institute of Geotechnical Engineering, Southeast University, Nanjing 210096, China. Post-Doctoral Fellow, Department of Civil and Environmental Engineering, Hong Kong University of Science and Technology, Hong Kong SAR, China. Email: wuhaoliang@ust.hk

Fei Jin

Assistant Professor, School of Engineering, University of Glasgow, Glasgow G12 8QQ, UK. Email: fei.jin@glasgow.ac.uk

Yan-Jun Du*

Professor, Jiangsu Key Laboratory of Urban Underground Engineering & Environmental Safety, Institute of Geotechnical Engineering, Southeast University, Nanjing 210096, China. Tel.: +862583793729; Fax: +862583795086,

*Corresponding author, Email: duyanjun@seu.edu.cn

Revised Manuscript Submitted to

Journal of Zhejiang University-SCIENCE A (Applied Physics & Engineering)

Abstract

The strength and hydraulic conductivity of vertical cutoff walls consisting of reactive magnesia-activated ground granulated blast furnace slag (GGBS), bentonite and soil (MSB) have been investigated in previous studies. However, there has been little comprehensive study of the influence of wet-dry cycles on the mechanical and microstructural properties of MSB backfills. In this paper, the durability of MSB backfills when exposed to wet-dry cycles is investigated. The variations in mass change, dry density, pH value, pore size distribution and mineralogy are discussed. The results show that the mass change of Ordinary Portland Cement (OPC)-based and MSB backfills increases with respect to wet-dry cycles. The MSB backfills exhibit up to 8.2% higher mass change than OPC-based ones after ten wet-dry cycles. The dry density, pH value and unconfined compressive strength of MSB backfill decrease with the increasing number of wet-dry cycles. Increasing the GGBS-MgO content from 5% to 10% in MSB backfills results in 2.1 - 2.3 times higher strength, corresponding to a reduction of 2% - 12% in cumulative pore volume; while increasing the bentonite content slightly reduces the strength of MSB mixtures, corresponding to an increase of cumulative pore volume by 4.6% - 7.9%. The hydrotalcite-like phases and C-S-H are the primary hydration products in MSB backfills. Moreover, the continuous wet-dry cycles resulte in the precipitation of calcite ($CaCO_3$) and nesquehonite ($MgCO_3 \cdot 3H_2O$).

Keywords: Cutoff wall; reactive MgO-activated GGBS; durability; wet-dry cycles; carbonation

1. Introduction

The soil-cement-bentonite (SCB) cutoff wall has been widely used worldwide in remediation projects for contaminated sites (Ryan and Day 2002; Opdyke and Evans 2005; Ruffing and Evans 2014). Such walls have been mainly used to interrupt the pollution pathway and to isolate the contaminant source from a vulnerable receptor (Joshi et al. 2008; Soga and Joshi 2015; Du et al. 2015; Yang et al. 2018 and 2019). As compared to soil-bentonite (SB) and cement-bentonite (CB) cutoff walls, SCB walls possess adequate strength to carry foundation loads. They have the additional economic merit of the reuse of site-excavated soils (Ryan and Day 2002; Opdyke and Evans 2005). In CB and SCB walls, Ordinary Portland cement (OPC) is the primary cementitious material used, and is associated with intensive CO_2 emissions (0.95 t/t OPC) and consumption of raw materials (Benhela et al. 2013). In recent years, many industrial by-products such as ground granulated blast furnace slag (GGBS) and fly ash have become popular as partial substitutions for OPC in geotechnical applications (Jefferis 2012; Lam and Jefferis, 2017; Arulrajah et al. 2017a; Arulrajah et al. 2017b; Wu et al. 2019). For example, replacing OPC with GGBS in the cutoff wall backfill has been applied extensively in the UK (Jefferis 2012). It has significant environmental and economic benefits, marginally affects the q_u (sometimes with enhancement), slightly decreases pore water pH and notably decreases hydraulic conductivity in the long term (Wu et al. 2019).

Compared to OPC, using reactive MgO as the activator for GGBS has many potential technical benefits, in particular for soil remediation applications. The main

hydration products in reactive MgO-activated GGBS are calcium silicate hydrate (C-S-H), hydrotalcite and brucite ($Mg(OH)_2$, if MgO is excessive) (Du et al. 2016; Jin et al. 2015; Jin and Al-Tabbaa 2014a; Wang et al. 2016; Yi et al. 2013). Due to the absence of highly soluble portlandite with a high equilibrium pH value (~12.5) and the formation of the above-mentioned products with excellent adsorptive capacities, MgO-GGBS blends have shown superiority over OPC for contaminant immobilization in a number of laboratory studies and field trials (Du et al. 2016; Jin et al. 2015; Jin et al. 2016; Jin and Al-Tabbaa, 2014a and b; Wang et al. 2016).

Recently, this novel cement has been applied to form an innovative cutoff wall backfill material, together with bentonite and site sandy soil (MSB) (Wu et al. 2019). The unconfined compressive strength (q_u) and hydraulic conductivity (k_w) of the proposed backfill permeated with tap water are in the range of 230 - 520 kPa and 1.1×10^{-10} - 6.3×10^{-10} m/s at 90-day-curing, respectively, complying well with the commonly adopted design limits ($q_u \geq 100$ kPa and $k_w \leq 1.0\times10^{-8}$ m/s) (ICE 1999; Ryan and Day 2002;). More importantly, this backfill showed excellent durability under exposure to sodium sulfate (Na_2SO_4) or lead-zinc (Pb-Zn) solutions (Wu et al. 2019). Environmental and cost assessments demonstrated that this innovative MSB backfill material reduced CO_2 emissions by 85% with ~15.3% - 16.9% lower cost when compared with OPC-based SCB backfills.

In a scenario of cutoff wall installations, the groundwater levels at each side of the barrier may fluctuate over time (Evans 1991; Ross and Beljin 1998). The potential changes in the q_u and k_w of the cutoff wall exposed to cyclic wet-dry actions have been

89 recognized as a medium- to long-term performance concern (Malusis et al., 2011;
90 National Research Council, 2007; Soga and Joshi, 2015). For CB and SCB walls,
91 noticeable cracks were observed due to shrinkage in the drying phase (Soga and Joshi
92 2015), which would lead to the increase of k_w by 2 - 3 orders (Joshi et al., 2009).
93 Previous studies also illustrated that the q_u of MgO-GGBS stabilized kaolin clay
94 reduced dramatically with increasing wet-dry cycles (Du et al., 2016). Thus, it is
95 necessary to evaluate the durability of the innovative MSB backfill under wet-dry
96 cycles.

97 This paper aims to investigate the effect of wet-dry cycles on the durability of
98 innovative MSB backfill. A series of laboratory tests, including mass change, dry
99 density, pH value, unconfined compression tests, Mercury Intrusion Porosimetry (MIP)
100 and X-ray diffraction (XRD) are performed in order to reveal the effects of wet-dry
101 cycles on the properties of MSB backfills.

102 **2. Materials and specimen preparation**

103 2.1 Solid materials

104 The backfill materials were prepared using Nanjing local soil, powdered sodium
105 activated calcium-bentonite, MgO and GGBS. The Nanjing local soil is classified as a
106 clayey sand based on the Unified Soil Classification System (ASTM 2017). The
107 commercial powdered sodium activated calcium-bentonite was provided by the
108 MuFeng mineral processing plant in Zhenjiang, China. GGBS and MgO used in this
109 study were obtained from Nanjing and Jinan, China, respectively. The physicochemical
110 properties for the site soil and bentonite are shown in **Table 1**. The moisture and specific

gravity were measured according to ASTM D2216 (ASTM, 2010a) and ASTM D4318 (ASTM, 2010b), respectively. The pH was measured by ASTM D4972 (ASTM, 2018a) using a pH meter HORIBAD-54. The cation exchange capacity was measured as in ASTM D7503 (ASTM, 2010c). The specific surface area was measured by nitrogen adsorption using a Physisorption Analyzer ASAP2020 according to (Cerato and Lutenegger, 2002). The medium reactivity MgO (reactivity is 102 s, determined by the acetic acid test according to Shand (2006)) was selected due to its appropriate reactivity and cost (Wu et al., 2018a and b; Jin and Al-Tababa, 2014c). The chemical compositions of the soil, GGBS and MgO used for this study are shown in **Table 2**, as measured by X-ray fluorescence (XRF) (ARL™ SMS-2000).

Table 1. Physicochemical properties of the local sandy-clay and bentonite

Index	Values			
	clayey sand	bentonite	GGBS	MgO
Moisture, (%)	4.81	11.2	-	-
pH (liquid to solid ratio at 1)	7.32	8.6	10.96	10.53
Specific gravity, G_s	2.62	2.66	-	-
Plastic limit, w_P (%)	-	55	-	-
Liquid limit, w_L (%)	-	103	-	-
Grain size distribution (%)				
Clay (<0.002 mm) [a]	5.62	99	-	-
Silt (0.002-0.075 mm) [a]	14.18	1	-	-
Sand (0.075-2 mm) [b]	80.20	-	-	-
Specific surface area, SSA (m^2/g)	-	378.5	0.29	28.02
Exchangeable cation (cmol/kg)				
Ca^{2+}		22.74		
Mg^{2+}		1.41		
Na^{+}		53.39		
K^{+}		0.53		
Sum		78.07		

[a] Measured using a laser particle analyzer Mastersizer 2000 (Malvern Instruments Ltd., UK)

[b] Measured with standard #10 - #200 sieves

Table 2. Chemical compositions of the clayed sand, OPC, GGBS and MgO (by wt%) used in this study determined by XRF

Oxides	Clayey sand	OPC	GGBS	MgO
CaO	0.41	49.75	34.00	0.23
Al_2O_3	35.76	10.87	17.90	0.28
MgO	0.06	2.26	6.02	92.95
K_2O	0.15	0.75	0.64	0.01
SiO_2	48.73	22.6	34.3	0.28
Fe_2O_3	6.13	3.50	1.02	-
SO_3	0.07	3.84	1.64	0.45
MnO	0.11	0.24	0.28	0.01
Loss of ignition (%)	8.58	6.19	4.20	5.79

2.2 Backfill mix design and specimen preparation

Table 3 shows the mix proportions of the studied backfills. The MgO to GGBS ratio was 1:9 to achieve good strength and the lowest hydraulic conductivity based on preliminary studies (Jin et al., 2015; Wu et al., 2018a; Wu et al., 2019). The binder (OPC or GGBS-MgO) dosages (by weight of dry soil) ranged from 2.5% to 12.5% based on a review of previous studies (**Fig. 1**) as reported in Wu et al. (2019), which included both field and lab test results of SCB cutoff walls. Furthermore, since natural high-quality Na-bentonite in China is scarce, in practice engineers usually prefer to choose a higher dosage (≥5%) of sodium activated calcium-bentonite. The raw solid materials, including the clayey sand, powdered sodium activated calcium-bentonite, OPC or MgO and GGBS were weighed and mixed in a 2-L Hobart stainless steel mixer at 30 rpm for 5 min. It should be noted that the backfill specimens were prepared by mixing the non-prehydrated bentonite with sandy soil-OPC or sandy soil-GGBS-MgO mixture. Then the predetermined amount of tap water (pH = 6.8; *EC* = 3.3 μS/cm) was added and mixed at 60 rpm for 10 min to achieve homogeneity with the same slump value (150 ± 5 mm) (Wu et al., 2019). In the OPC-based backfill, the content of the

GGBS used in this study was 80% replacement of OPC, which was reported to exhibit the lowest k_w and highest q_u (Opdyke and Evans, 2005). The mixtures were poured into cylindrical moulds with sizes of Φ50 × H100 mm and cured for 90 days under standard curing conditions (T = 20 ± 2 °C, RH = 95%).

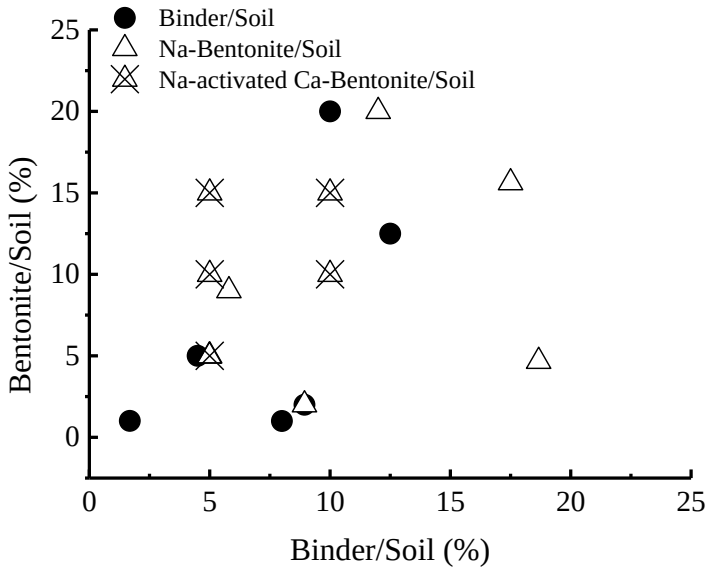

Fig. 1 Summary of bentonite/soil and binder/soil ratios in SCB cutoff wall backfill mix designs reported in previous studies (adapted from Wu et al., 2019)

Table 3. Mix design for the backfills used in this study (wt%)

Category ID	Code	Clayey sand	Bentonite	OPC	GGBS	MgO
C	C5	100	-	5	-	-
CB	C5B5	100	5	5	-	-
	C10B10	100	10	10	-	-
CSB	CS5B5	100	5	1	4	-
	CS10B10	100	10	2	8	-
MSB	MS5B5	100	5	-	4.5	0.5
	MS5B10	100	10	-	4.5	0.5
	MS5B15	100	15	-	4.5	0.5
	MS10B10	100	10	-	9	1
	MS10B15	100	15	-	9	1

3. Laboratory testing program

The 90-day cured specimens were subjected to wet-dry cycles according to Kamon et al. (1993). For each drying cycle, the specimens were stored in an oven (30 °C) for

48 h, followed by soaking in the distilled water with a temperature of 20 °C for 24 h. The drying temperature was set as 30 °C to represent the typical average temperature of hot seasons in the southeast regions of China and to minimize the effect of accelerated slag hydration due to temperature rise (Du et al., 2016). The duration of such a wet-dry cycle was three days and it was repeated for ten cycles.

After the i^{th} wet or dry cycle, the mass change (MC) of the specimen is calculated by Equation (1):

$$MC=(m_0-m_i)/m_0 \quad (1)$$

where m_0 = initial mass of the specimen measured prior to the wet-dry cycles, and m_i = mass of the sample measured immediately after the i^{th} drying cycle.

The densities of the specimens were measured in triplicate as in ASTM D7263 (2018b), and average values were reported. The specimens were subjected to UCT as in ASTM D4219 (ASTM, 2008) with a strain rate of 1%/min. Fragments from the core of the broken UCT specimens were air-dried, crushed and passed through a 2-mm sieve. Ten grams of the sieved soil and 10 ml of distilled water (water to solid ratio = 1: 1) were poured into a glass container to determine the pore water pH. The pH values of the supernatant were measured by a HORIBA D-54 pH meter and the average value was reported.

After the 10^{th} wet-dry cycle, dry specimens were prepared to conduct MIP and XRD tests. Briefly, ~1 cm^3 sample was collected from the specimen's core by a stainless steel knife and frozen in liquid nitrogen. The frozen sample was dried in a vacuum chamber at -80°C. The MIP tests were conducted according to ASTM D4404 (2010d)

using an Auto Pore IV 9510 mercury intrusion porosimeter to determine the pore size distribution. Prior to XRD analysis, the dry specimens were ground and sieved to < 0.075 mm. The XRD spectra were obtained using a RigakuD/Max-2500 spectrometer using a Cu-Kα source with a wavelength of 1.5405 Å. The instrument was operated at 40 kV and 20 mA. A step size of $2\theta = 0.02^{\circ}$ and a scanning speed of 5 s/step were used over a range of 2θ from 10° to 50°in the step scan mode.

4. Results and Discussion

4.1 Mass change and visual inspection of physical integrity

Fig. 2 (a) and **(b)** present the variations in mass change with the wet-dry cycles for the OPC-based and MSB backfills. It can be seen that the mass changes of the two types of backfill increase with respect to the wet-dry cycles. Increasing the binder content (GGBS-MgO) in the MSB backfills reduces mass change (by ~ 9.0 - 11%) (i.e., comparing MS10B10 and MS10B15 with MS5B10 and MS5B15, respectively). **Fig. 2 (b)** also indicates that increasing the bentonite content from 5% to 15% leads to a higher mass change for the MSB backfills. This is attributed to the fact that higher bentonite content (i.e., MS5B15) is more sensitive to the loss of water as compared to MS5B5 and MS5B10, which would develop matrix suction and increase the shrinkage in the backfills in the drying stages (Nahlawi and Kodikara, 2006; Rowe et al., 2011; Tang et al., 2011). However, the binder and bentonite contents show no significant impact on the OPC-based backfills as shown **Fig. 2 (a)**. After the last wet-dry cycle, the mass changes in MSB backfills reach approximately 12 - 19%, and are slightly higher than

those for the OPC-based backfills. Meanwhile, the mass change is much higher in MSB than OPC at the wetting stage; the difference is much smaller at the drying stage. This may imply that the water absorption potential of the bentonite in MSB mixtures is better preserved than that in OPC-based mixtures. It was also found that spalling and macro-cracks started to develop at the 4^{th} - 6^{th} cycles and were exacerbated with each wet-dry cycle, as shown in **Fig. 3**.

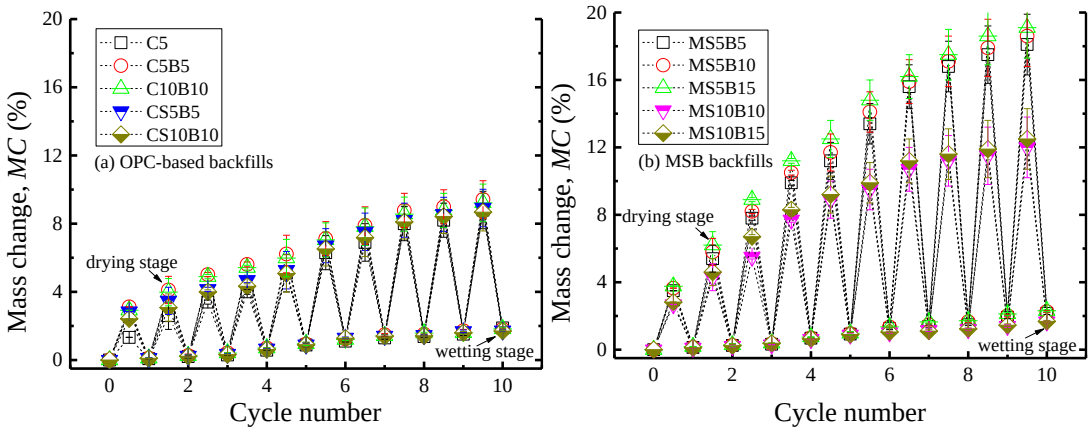

Fig. 2 Variations in mass change with wet-dry cycles for (a) OPC-based and (b) MSB backfills

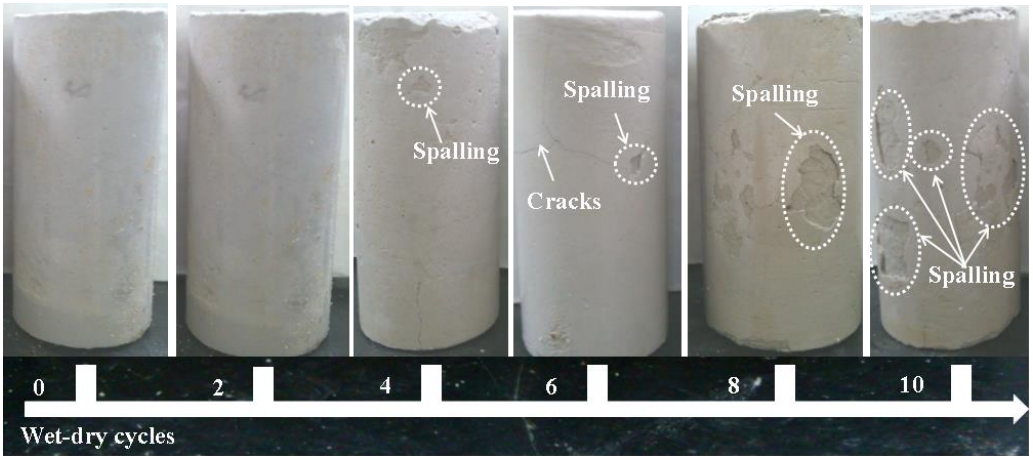

Fig. 3 Photos showing the physical integrity of MSB backfills during wet-dry cycling

4.2 Dry density

Fig. 4 shows the variations of average values and standard deviations (STD) of dry densities with wet-dry cycles for OPC-based and MSB backfills. The dry densities

of OPC-based and MSB backfills are 1.34 - 1.39 g/cm^3 and 1.31 - 1.35 g/cm^3 after the 10th wet-dry cycles, respectively. For all backfills, the dry density decreases slightly with the wet-dry cycles, which is consistent with the mass change evolution as shown in **Fig. 2**. For the identical binder and bentonite content, it is found that the dry density of MSB backfills (i.e., M5B5) is higher than that of OPC-based backfills (i.e., C5B5 and CS5B5) after being exposed to ten wet-dry cycles. This may be attributed to the fact that the C-S-H gels formed in GGBS-MgO have a lower Ca/Si ratio compared to those formed in OPC, leading to higher shrinkage during the drying process (Du et al., 2016; Jin et al., 2014b). At the same bentonite content in MSB backfills, the increase of GGBS-MgO content has only a slight impact on the dry density (i.e., comparing MS10B10 and MS10B15 with MS5B10 and MS5B15, respectively) whereas the dry density significantly decreases as the bentonite content increases from 5% to 15% at the identical GGBS-MgO content (i.e., comparing MS5B5 with MS5B10 and MS5B15) after ten wet-dry cycles.

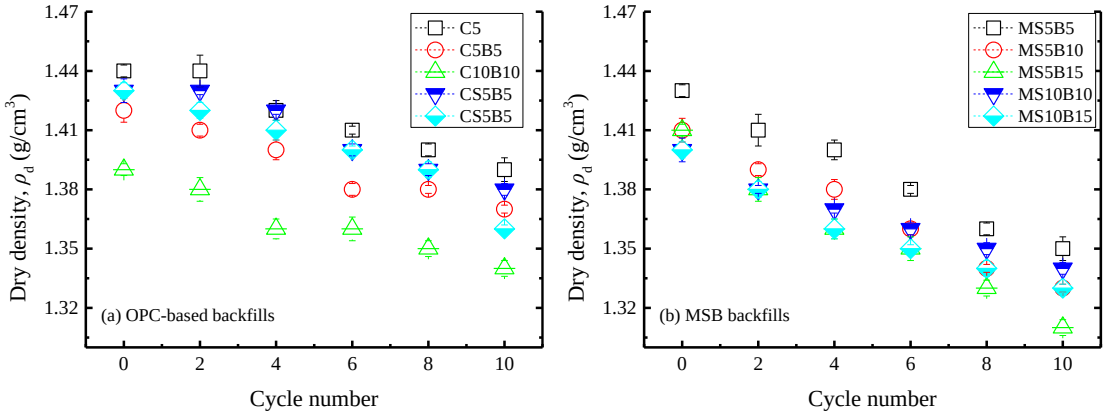

Fig 4. Dry density values for backfills after wet-dry cycles

4.3 pH value

Fig. 5 depicts the variations in the soil pH values with the wet-dry cycles for OPC-

based and MSB backfills. It can be observed that the pH for all backfills gradually decreases with increasing wet-dry cycles. This is attributed to the leaching of alkaline substances (i.e., Ca^{2+}) from the backfills when exposed to wetting. After ten wet-dry cycles, the pH of OPC-based and MSB backfills are 10.9 - 12.3 and 9.8 - 10.8, respectively. At the same binder and bentonite contents, the pH values of MSB backfills are much lower than those of OPC-based backfills either before or after the wet-dry cycles. For instance, the pH values for 5% GGBS-MgO in MSB backfills (i.e., MS5B5 and CS5B5) are approximately 0.5 - 1.2 lower than those for 5% OPC-based backfills (i.e., C5B5 and CS5B5) after ten wet-dry cycles. Increasing the bentonite content in MSB backfills reduces the pH values by 0.4 and 0.2 unit at 5% and 10% binder contents (i.e., comparing MS5B10 and MS10B10 with MS5B15 and MS10B15, respectively) after ten wet-dry cycles. Increasing the GGBS-MgO content results in higher pH, while increasing the bentonite content decreases the pH value in the MSB mixtures.

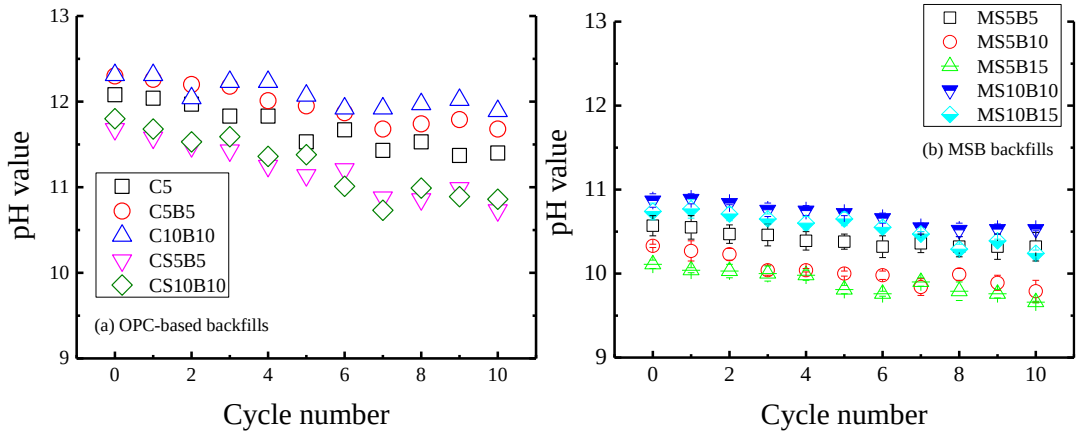

Fig. 5 Variations in pH with wet-dry cycles for (a) OPC-based and (b) MSB backfills

4.4 Unconfined compressive strength

Fig. 6 shows the evolution of q_u for the OPC-based and MSB specimens. It is found that q_u values of the two types of backfill decrease with increasing wet-dry cycles. After

255 ten wet-dry cycles, the q_u values of the OPC-based and MSB backfills are 400 – 540
256 kPa and 180 – 420 kPa, respectively. The decreased q_u is attributed to the gradually
257 dissolved Ca^{2+} from the OPC-based and MSB matrices exposed to wetting conditions
258 (Du et al., 2016; Shen et al., 2008). As the pH decreases to below 10.8 (**Fig. 5**), the
259 partial destruction of C-S-H gels in the MSB backfill matrix also leads to lower q_u
260 when compared to OPC-based backfills (**Fig. 6**). For the MSB backfills, the q_u of 10%
261 GGBS-MgO in MSB backfills (i.e., MS10B10 and MS10B15) is 2.1 - 2.3 times higher
262 than that of 5% GGBS-MgO (i.e., MS5B10 and MS5B15). It is also observed that
263 increasing the bentonite content at the same binder content slightly reduces the strength
264 of MSB mixtures, and that is consistent with the higher mass change and lower dry
265 density shown in **Fig. 2** and **Fig. 4**.

266 The strength loss (*SL*) and cumulative strength loss (*CSL*) is computed by
267 Equations (2) and (3).

268 $$SL_i=(q_{u0}-q_{ui})/q_{u0} \quad (2)$$

269 $$CSL=\sum_{i=0}^{10} SL_i \quad (3)$$

270 where q_{u0} = initial unconfined compressive strength of the specimen measured prior to
271 the wet-dry cycles, and q_{ui} = mass unconfined compressive strength of the sample
272 measured immediately after the i^{th} wet-dry cycle.

273 It can be observed that the *CSL* for 5% GGBS-MgO backfills (i.e., MS5B10 and
274 MS5B15) is 35% - 47% higher than that of 10% GGBS-MgO (i.e., MS10B10 and
275 MS10B15) as shown in **Fig. 7**. Furthermore, *CSL* decreases by 2.7% and 6.4% for 5%
276 and 10% GGBS-MgO in MSB backfills, respectively, as the bentonite increases from

10% to 15%. Thus, the impact of wet-dry cycles on MSB backfills is greater than on OPC-based backfills. This phenomenon might be attributed to: (i) a lower Ca/Si ratio of C-S-H in MSB backfills as compared to that formed in the OPC-based backfills, which is more prone to shrinkage under the drying process, resulting in micro-cracking of the matrix (Jin et al., 2014b) and (ii) a larger amount of uncombined water remaining in the MSB backfills due to the better preserved bentonite swelling/shrinkage behavior (Wu et al., 2019), which is prone to evaporation and leads to substantial shrinkage cracking upon drying, resulting in greater strength loss.

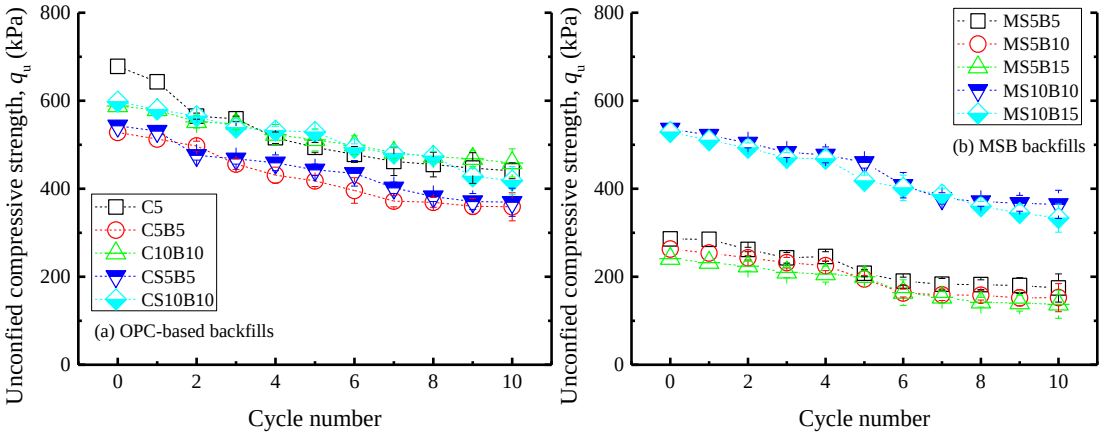

Fig. 6 Effective of wet-dry cycles on q_u for (a) OPC-based and (b) MSB backfills

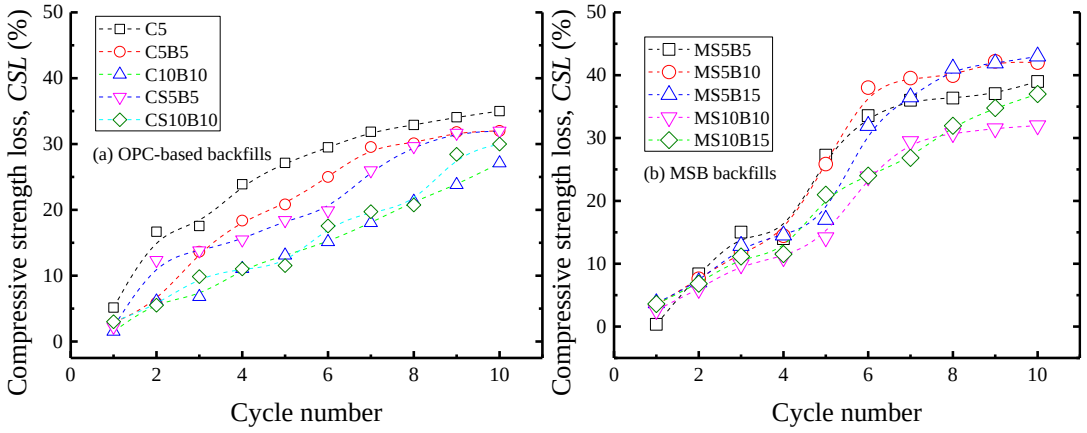

Fig. 7 Effect of wet-dry cycles on cummulative strength loss for (a) OPC-based and (b) MSB backfills

4.5 Pore size distribution

To investigate the evolution in pore profiles of MSB backfills with respect to wet-

292 dry cycles, MIP tests are conducted. **Fig. 8 (a)** shows the cumulative pore volumes of
293 the MSB backfills after ten wet-dry cycles. At the same bentonite content, the
294 cumulative pore volumes of MS5B10 and MS5B15 are found to decrease by 12% and
295 2% as compared with MS10B10 and MS10B15. At 5% GGBS-MgO content, increasing
296 the bentonite content from 5% to 10% and 15% increases the cumulative pore volume
297 by 4.6% and 7.9%, respectively. The results for the pore profiles are consistent with the
298 observed trends for q_u and mass change as shown in **Fig. 6 (b) and Fig 2 (b).**

299 **Fig. 8 (b)** shows the volumes of the pores in different size ranges: <0.01 μm (intra-
300 aggregate), 0.01 – 10 μm (inter-aggregate) and >10 μm(air pores) respectively. This
301 classification of pore sizes is suggested by Horpibulsuk et al., (2010) and Xia et al.,
302 (2018 and 2019) for the OPC stabilized silty clay. Regardless of the binder content, the
303 proportions of air pores and inter-aggregate pores decrease but intra-aggregate pores
304 increase as the bentonite content increases from 5% to 15%. At the same bentonite
305 content, increasing the binder content decreases the proportions of pores in each
306 category (i.e., comparing MS5B10 and MS10B10 with MS5B15 and MS10B15). As
307 reported in previous studies (Collins and Sanjayan, 2000; Du et al., 2014 and 2016), a
308 larger volume of inter-aggregate pores can lead to higher drying-initiated capillary
309 tension forces and greater shrinkage potential in the matrix. Thus, the MS10B10
310 mixture shows the highest q_u and least mass change among all the MSB backfills as
311 shown in **Fig. 6** and **Fig. 2**.

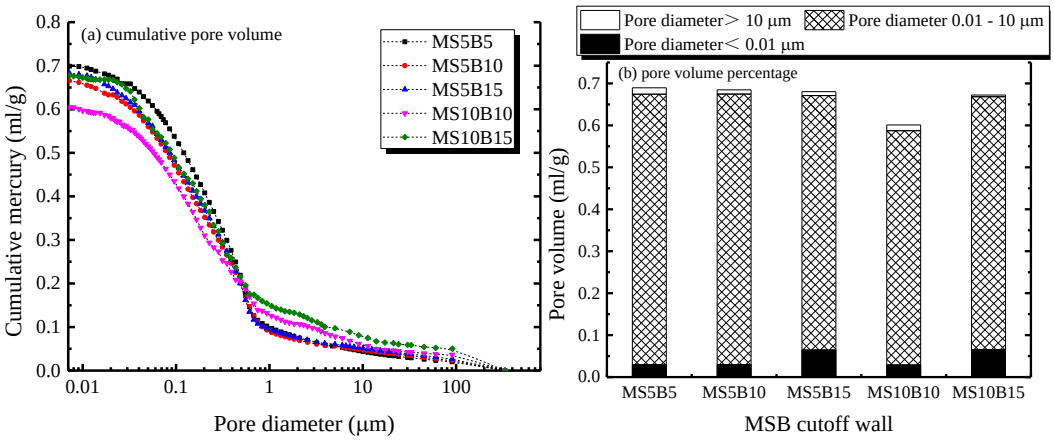

Fig. 8 The (a) cumulative pore volume and (b) pore volume percentage of MSB backfills after 90 days standard curing and subjected to ten wet-dry cycles

4.6 X-ray diffraction

XRD tests were conducted on the MSB specimens before and after ten wet-dry cycles to investigate the evlolution of the phase assemblage in the mixtures as presented in **Fig. 9 (a)** and **(b)**. The characteristic peaks of hydrotalcite ($Mg_6Al_2(OH)_{16}CO_3{\cdot}4H_2O$)-like phases (Ht) were found at $2\theta \approx 12.5°$ and 24.0°, agreeing well with previous findings (Jin et al., 2014a). In addition, two broad peaks ascribed to C-S-H were detected at $2\theta \approx 23.0°$, 30.0°, 31.6° and 37.5°, and were the result of the reaction between released silicate species and Ca from GGBS (Wu et al., 2019; Jin et al., 2014a and b). The C-S-H gels and hydrotalcite can improve the strength and hydraulic performance in MSB cutoff wall applications. Further, hydrotalcite has contaminants (e.g., lead and zinc) with a high capacity for adsorbtion and which therefore can enhance the chemical compatibility of the backfills exposed to contaminated underground conditions. The higher intensity of Ht and C-S-H are observed in 10% GGBS-MgO (i.e., MS10B10 and MS10B15) as compared with 5% GGBS-MgO (i.e., MS5B5, MS5B10 and MS10B15), and result in higher q_u (**Fig. 6**)

and lower mass change (**Fig. 2**). The characteristic peak of quartz (SiO_2) has been detected at $2\theta \approx 21.6°$ in the local clayey sand. The characteristic peaks of calcium hydroxide ($Ca(OH)_2$) have been detected at $2\theta \approx 19.0°$, 34.5° and 46.5°, from the leaching of Ca^{2+} from GGBS and C-S-H. The leaching of Ca^{2+} will lead to the decrease of pH value as illustrated in **Fig. 5**. Nesquehonite ($MgCO_3{\cdot}3H_2O$) is found in the backfills after ten wet-dry cycles, as the peaks at $2\theta \approx 14.2°$ and 41.0°) agree with those reported by Wu et al., (2018b) and Ruan et al. (2019) It is formed by the dissolved Mg^{2+} from the MSB backfills and dissolved CO_2 from the atmosphere. Similarly the leached Ca^{2+} from the GGBS and C-S-H may react with dissolved atmospheric CO_2 to form calcite. Nevertheless, the strongest calcite peak ($2\theta \approx 30.0°$) overlaps with that of C-S-H, which prevents its identification via XRD in this study.

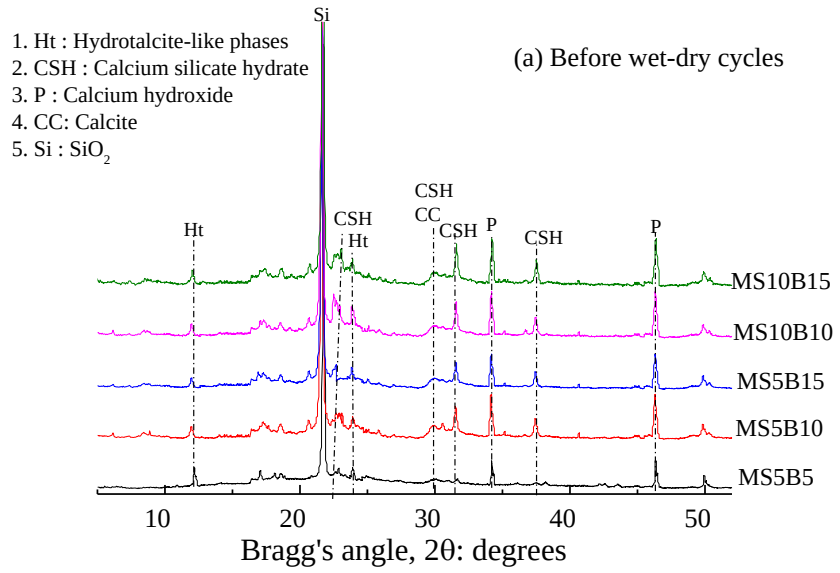

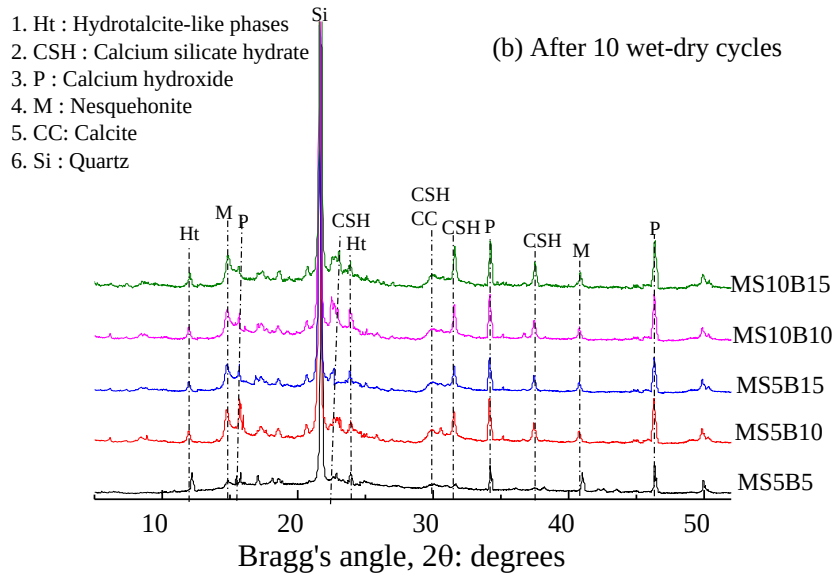

Fig. 9 X-ray diffractograms of the 90-day cured MSB backfills before (a) and after (b) wet-dry cycles: Ht: Hydrotalcite-like phases, CSH: Calcium silicate hydrate, P: Calcium hydroxide, M: Nesquehonite, CC: Calcite, Si: Quartz

5. Limitations of current study

This study reveals that the MSB mixture is more sensitive to a fluctuating groundwater condition than OPC-based backfills. This might be attributed to the hydration products (C-S-H with lower a Ca/Si ratio) and microstructure (refined pores) formed in alkali-activated GGBS paste as compared to OPC-based backfills (Du et al., 2015). Nevertheless, the unconfined compressive strength values of MSB mixtures are still above the commonly adopted design limits ($q_u \geq 100$ kPa) after ten wet-dry cycles. The much lower pH values of pore water in MSB mixtures have much weaker impact on the chemical stability of montmorillonite in bentonite as compared to OPC-based backfills (Wu et al., 2019). In addition, the use of a large amount of industrial waste gives the MSB mixture better sustainability than the OPC-based backfills.

Admittedly, for a full understanding of the long-term durability of the MSB backfills after wet-dry cycles, the wet-dry aging could be correlated with real time for a quantitative simulation (Shen et al., 2018 and 2019). Further investigations are

360 warranted to elucidate the change of hydraulic conductivity, hydration products, and
361 micrsotructures of the backfills under the various extreme environmental stresses that
362 might be encountered in the field.

363 **6. Conclusions**

364 A comprehensive laboratory testing program was conducted to reveal the effects
365 of wet-dry cycles on the properties of MSB backfills and the following conclusions can
366 be drawn:

367 (1) The mass change of OPC-based and MSB backfills increased with respect to
368 the wet-dry cycles. The MSB backfills exhibited 1.1% - 2.1% higher mass change than
369 OPC-based ones after ten wet-dry cycles. Increasing the GGBS-MgO content reduced
370 9.0 - 11% mass change but increasing the bentonite content increased mass change in
371 MSB backfills. The threshold cycle numbers for spalling and macro-cracks occurring
372 in MSB backfills were found to be in the 4^{th}- 6^{th} cycles.

373 (2) The dry density and pH of OPC-based and MSB backfills gradually decreased
374 with increasing wet-dry cycles. For the identical binder (OPC and GGBS-MgO) and
375 bentonite contents, the mass change of MSB backfills was higher than in OPC-based
376 backfills, while the pH was much lower.

377 (3) The unconfined compressive strength of OPC-based and MSB backfills
378 decreased with increasing wet-dry cycles. The strength values of the MSB backfills
379 with 10% GGBS-MgO were 2.1 - 2.3 times higher than those with 5% GGBS-MgO,
380 while increasing the bentonite content slightly reduced the strength. The cumulative
381 strength loss of MSB backfills was more notable than that for OPC-based backfills.

382 (4) Increasing the GGBS-MgO content from 5% to 10% reduces by 2% - 12% the
383 cumulative pore volume, while increasing the bentonite content from 5% to 15%
384 increases the cumulative pore volume by 4.6% - 7.9%.
385 (5) The hydrotalcite-like phases and C-S-H were found to be the primary hydration
386 products in the MSB backfills both before and after the wet-dry cycles. The wet-dry
387 cycles accelerated the leaching of earth alkali ions, which react with the dissolved CO_2
388 from the atmosphere to form calcite ($CaCO_3$) and nesquehonite ($MgCO_3 \cdot 3H_2O$) in
389 MSB mixtures.
390

391 **Acknowledgments**

392 This study was finanically supported by the National Key Research and
393 Development Programme (Grant Nos. 2018YFC1803100 and 2018YFC1802300), the
394 National Natural Science Foundation of China (Grant No. 41877248), and the Primary
395 Research & Development Plan of Jiangsu Province (Grant No. BE2017715)..
396

References

Arulrajah, A., Kua, T. A., Horpibulsuk, S., et al., 2017. Recycled glass as a supplementary filler material in spent coffee grounds geopolymers. *Construction and Building Materials*, 151, 18-27. https://doi.org/10.1016/j.conbuildmat.2017.06.050

Arulrajah, A., Kua, TA., Suksiripattanapong, C., Horpibulsuk, S., et al., 2017. Compressive strength and microstructural properties of spent coffee grounds-bagasse ash based geopolymers with slag supplements. *Journal of Cleaner Production*, 162, 1491-1501. https://doi.org/10.1016/j.jclepro.2017.06.171

ASTM. 2008. Standard test method for unconfined compressive strength index of chemical-grouted soils. ASTM D4219. West Conshohocken, USA.

ASTM. 2010a. Standard Test Methods for Laboratory Determination of Water (Moisture) Content of Soil and Rock by Mass. ASTM D2216. West Conshohocken, USA.

ASTM. 2010b. Standard Test Methods for Liquid Limit, Plastic Limit, and Plasticity Index of Soils. ASTM D4318, West Conshohocken, USA.

ASTM. 2010c. Standard Test Method for Measuring the Exchange Complex and Cation Exchange Capacity of Inorganic Fine-Grained Soils. ASTM D7503. West Conshohocken, USA.

ASTM, 2010d. Standard test method for determination of pore volume and porevolume distribution of soil and rock by mercury intrusion porosimetry. ASTM D4404.

West Conshohocken, USA.

ASTM. 2014. Standard Test Methods for Specific Gravity of Soil Solids by Water Pycnometer. ASTM D4813. West Conshohocken, USA.

ASTM. 2017. Standard practice for classification of soils for engineering purposes (Unified Soil Classification System). ASTM D2487. West Conshohocken, USA.

ASTM. 2018a. Standard Test Method for pH of Soils. ASTM D4972. West Conshohocken, USA.

ASTM. 2018b. Standard test methods for laboratory determination of density (unit weight) of soil specimens. ASTM D7263. West Conshohocken, USA.

Benhelal, E., Zahedi, G., Shamsaei, E., and Bahadori, A. 2013. Global strategies and potentials to curb CO_2 emissions in cement industry. *Journal of Cleaner Production*, 51, 142-161. http://dx.doi.org/10.1016/j.jclepro.2012.10.049

Cerato, A. B., and Lutenegger, A. J. 2002. Determination of surface area of fine-grained soils by the ethylene glycol monoethyl ether (EGME) method. *Geotechnical Testing Journal*, 25(3), 315-321.

Collins, F., and Sanjayan, J. G. 2000. Effect of pore size distribution on drying shrinking of alkali-activated slag concrete. *Cement and Concrete Research*, 30, 1401–1406. https://doi.org/10.1016/s0008-8846(00)00327-6

Du, Y. J., Jiang, N. J., Liu, S. Y., et al., 2014. Engineering properties and microstructural characteristics of cement-stabilized zinc-contaminated kaolin. *Canadian Geotechnical Journal*, 51(3), 289-302.

https://doi.org/10.1139/cgj-2013-0177

Du, Y. J., Fan, R. D., Liu, S. Y., et al., 2015. Workability, compressibility and hydraulic conductivity of zeolite-amended clayey soil/calcium-bentonite backfills for slurry-trench cutoff walls. *Engineering Geology*, 195, 258-268. https://doi.org/10.1016/j.enggeo.2015.06.020

Du, Y. J., Bo, Y. L., Jin, F., et al., 2016. Durability of reactive magnesia-activated slag-stabilized low plasticity clay subjected to drying–wetting cycle. *European Journal of Environmental and Civil Engineering*, 20(2), 215-230. https://doi.org/10.1080/19648189.2015.1030088

Evans, J. C. 1991. Geotechnics of hazardous waste control systems. Foundation engineering handbook, 2nd Ed., H. Y. Fang. ed., Van Nostrand Reinhold Company, New York, N.Y. https://doi.org/10.1007/978-1-4757-5271-7_20

Horpibulsuk, S., Rachan, R., Chinkulkijniwat, A., et al., 2010. Analysis of strength development in cement-stabilized silty clay from microstructural considerations. *Construction and Building Materials*, 24(10), 2011-2021. https://doi: 10.1016/j.conbuildmat.2010.03.011

ICE (Institution of Civil Engineers). 1999. Specification for the construction of slurry trench cut-off walls as barriers to pollution migration. Thomas Telford, London. https://doi.org/10.1680/sftcostcw.26254

Jefferis, S. 2012. Cement-bentonite slurry systems. Grouting and deep mixing, L. F. Johnsen, D. A. Bruce, and M. J. Byle, eds., 1-24. Reston, VA, ASCE. https://doi.org/10.1061/9780784412350.0001

463 Jin, F., and Al-Tabbaa, A. 2014a. Characterisation of different commercial reactive
464 magnesia. *Advances in Cement Research*, 26(2), 101-113.
465 https://doi.org/10.1680/adcr.13.00004
466 Jin, F., Gu, K., and Al-Tabbaa, A. 2014b. Strength and drying shrinkage of reactive
467 MgO modified alkali-activated slag paste. *Construction and Building Materials*,
468 51, 395–404.
469 https://doi.org/10.1016/j.conbuildmat.2013.10.081
470 Jin, F., and Al-Tabbaa, A. 2014c. Evaluation of novel reactive MgO activated slag
471 binder for the immobilization of lead and zinc. *Chemosphere*, 117: 285-294.
472 https://doi.org/10.1016/j.chemosphere.2014.07.027
473 Jin, F., Gu, K. and Al-Tabbaa, A. 2015. Strength and hydration properties of reactive
474 MgO-activated ground granulated blastfurnace slag paste. *Cement and Concrete*
475 *Composites*, 57, 8-16.
476 https://doi.org/10.1016/j.cemconcomp.2014.10.007
477 Joshi, K., Soga, K., Ng, M. Y. A., et al., 2008. Durability Study of Eleven Years Old
478 Cement-Bentonite Cut-Off Wall Material. *GeoCongress 2008: Geotechnics of*
479 *Waste Management and Remediation*, 620-627. New Orleans, LA, ASCE.
480 https://doi.org/10.1061/40970(309)78
481 Joshi, K., Kechavarzi, C., Sutherland, K., et al., 2009. Laboratory and in situ tests for
482 long-term hydraulic conductivity of a cement-bentonite cutoff wall. *Journal of*
483 *Geotechnical and Geoenvironmental Engineering*, 136(4), 562-572.
484 https://doi:10.1061/(asce)gt.1943-5606.0000248

485 Kamon, M., Nontananandh, S., and Katsumi, T. 1993. Utilization of stainless-steel slag
486 by cement hardening. *Soils and Foundations*, 118–129.
487 https://doi.org/10.3208/sandf1972.33.3_118
488 Kitazume, M., and Terashi, M. 2002. The deep mixing method principle, design and
489 construction. Tokyo: Balkema.
490 Lam, C., and Jefferis, S. A.. 2017. Polymer Support Fluids in Civil Engineering, ICE
491 Publishing, One Great George Street, Thomas Telford Limited, London.
492 https://doi.org/10.1680/psfce.57869
493 Liu, L., A. Zhou, Y. Deng, Y. Cui, Z. Yu, and C. Yu. 2019. Strength performance of
494 cement/slag-based stabilized soft clays. *Construction and Building Materials*, 211,
495 909-918.
496 https://doi.org/10.1016/j.conbuildmat.2019.03.25
497 Ma, L., Xu, D., S. Wang, S., et al., 2019. Expansion inhibition of steel slag in asphalt
498 mixture by a surface water isolation structure. *Road Materials and Pavement*
499 *Design*, 1-15.
500 https://doi.org/10.1080/14680629.2019.1601588
501 Malusis, M. A., Yeom, S., and Evans, J. C. 2011. Hydraulic conductivity of model soil–
502 bentonite backfills subjected to wet–dry cycling. *Canadian Geotechnical Journal*,
503 48(8), 1198-1211.
504 https://doi.org/10.1139/t11-028
505 Nahlawi, H., and Kodikara, J. K. 2006. Laboratory experiments on desiccation cracking
506 of thin soil layers. *Geotechnical and Geological Engineering*, 24(6), 1641-1664.

https://doi.org/10.1007/s10706-005-4894-4

National Research Council. 2007. Assessment of the performance of engineered waste containment facilities. The National Academies Press, Washington, D.C. https://doi.org/10.17226/11930

Opdyke, S. M., and Evans, J. C. 2005. Slag-cement-bentonite slurry walls. *Journal of Geotechnical and Geoenvironmental Engineering*, 131(6), 673-681.

Owaidat, L. M., Andromalos, K. B., Sisley, J. L., et al., 1999. Construction of a soil-cement-bentonite slurry wall for a levee strengthening program. In Proceedings of the 1999 Annual Conference of the Association of State Dam Safety Officials, St. Louis, Mo. 10-13.

Ross, R. R., and Beljin, M. S. 1998. Evaluation of containment systems using hydraulic head data. *Journal of Environmental Engineering*, 124(6), 575-578. https://doi.org/10.1061/(asce)0733-9372(1998)124:6(575)

Rowe, R. K., Bostwick, L. E., and Take, W. A. 2011. Effect of GCL properties on shrinkage when subjected to wet-dry cycles. *Journal of Geotechnical and Geoenvironmental Engineering*, 137(11), 1019-1027. https://doi.org/10.1061/(asce)gt.1943-5606.0000522

Ruan, S., Qiu, J., Weng, Y., et al., 2019. The use of microbial induced carbonate precipitation in healing cracks within reactive magnesia cement-based blends. *Cement and Concrete Research*, 115, 176-188. https://doi.org/10.1016/j.cemconres.2018.10.018

Ruffing, D. G., and Evans J. C. 2014. Case Study: Construction and In Situ Hydraulic

529 Conductivity Evaluation of a Deep Soil-Cement-Bentonite Cutoff Wall". *In Proc.*,
530 *Geo-Congress 2014*, 1863-1848. Atlanta, Georgia, ASCE.
531 https://doi.org/10.1061/9780784413272.180
532 Ryan, C. R., and Day S. R. 2002. Soil-cement-bentonite slurry walls. In Deep
533 foundations 2002: an international perspective on theory, design,construction, and
534 performance (Geotechnical Special Publication). 713-727.
535 https://doi.org/10.1061/40601(256)51
536 Shand, M. A. 2006. The chemistry and technology of magnesia, John Wiley & Sons.
537 Shen, S. L., Han, J., and Du, Y. J. 2008. Deep mixing induced property changes in
538 surrounding sensitive marine clays. *Journal of Geotechnical and*
539 *Geoenvironmental Engineering*, 134,845–854.
540 https://doi.org/10.1061/(asce)1090-0241(2008)134:6(845)
541 Shen, Z. T., Pan, S. Z., Hou, D., et al., 2019. Temporal effect of MgO reactivity on the
542 stabilization of lead contaminated soil. *Environment international*, 131, 104990.
543 https://doi.org/10.1016/j.envint.2019.104990
544 Shen, Z. T., Hou, D., Xu, W. D., Zhang, et al., 2018. Assessing long-term stability of
545 cadmium and lead in a soil washing residue amended with MgO-based binders
546 using quantitative accelerated ageing. *Science of the Total Environment*, 643,
547 1571-1578.
548 https://doi.org/10.1016/j.scitotenv.2018.06.321
549 Soga, K., and Joshi K. 2015. Cement bentonite cutoff walls for polluted sites. In Proc.,
550 Coupled Phenomena in Environmental Geotechnics, Taylor and Francis Group,

149-165.
https://doi.org/10.1201/b15004-15

Tang, C. S., Shi, B., Liu, C., et al., 2011. Experimental characterization of shrinkage and desiccation cracking in thin clay layer. *Applied Clay Science*, 52(1-2), 69-77. https://doi.org/10.1016/j.clay.2011.01.032

Wang, F., Jin, F., Shen, Z., et al., 2016. Three-year performance of in-situ mass stabilised contaminated site soils using MgO-bearing binders. *Journal of Hazardous Materials*, 318, 302-307. https://doi.org/10.1016/j.jhazmat.2016.07.018

Wu, H. L., Jin, F., Bo, Y. L., et al., 2018a. Leaching and microstructural properties of lead contaminated kaolin stabilized by GGBS-MgO in semi-dynamic leaching tests. *Construction and Building Materials*, 172, 626-634. https://doi.org/10.1016/j.conbuildmat.2018.03.164

Wu, H. L., Zhang, D., Ellis, B. R., et al., 2018b. Development of reactive MgO-based Engineered Cementitious Composite (ECC) through accelerated carbonation curing. *Construction and Building Materials*, 191, 23-31. https://doi.org/10.1016/j.conbuildmat.2018.09.196

Wu, H. L., Jin, F., Ni, J. et al., 2019. Engineering properties of vertical cutoff walls consisting of reactive magnesia-activated slag and bentonite: workability, strength and hydraulic conductivity. *Journal of Materials in Civil Engineering*. 31(11), 04019263. https://doi.org/10.1061/(ASCE)MT.1943-5533.0002908

573 Xia, W. Y., Du, Y. J., Li, F. S., et al., 2019a. In-situ solidification/stabilization of heavy
574 metals contaminated site soil using a dry jet mixing method and new
575 hydroxyapatite based binder. *Journal of Hazardous Materials*, 369, 353-361.
576 https://doi.org/10.1016/j.jhazmat.2019.02.031
577 Xia, W. Y., Du, Y. J., Li, F. S., et al., 2019b. Field evaluation of a new hydroxyapatite
578 based binder for ex-situ solidification/stabilization of a heavy metal contaminated
579 site soil around a Pb-Zn smelter. *Construction and Building Materials*, 210, 278-
580 288.
581 https://doi.org/10.1016/j.conbuildmat.2019.03.195
582 Yang, Y. L., Reddy, K. R., Du, Y. J., et al., 2018. Short-term hydraulic conductivity
583 and consolidation properties of soil-bentonite backfills exposed to CCR-impacted
584 groundwater. *J Geotech Geoenviron Eng*, 144(6), 04018025.
585 https://doi.org/10.1061/(asce)gt.1943-5606.0001877
586 Yang, Y. L., Reddy, K. R., Du, Y. J., et al., 2019. Retention of Pb and Cr (VI) onto slurry
587 trench vertical cutoff wall backfill containing phosphate dispersant amended Ca-
588 bentonite. *Applied Clay Science*, 168, 355-365.
589 https://doi.org/ 10.1016/j.clay.2018.11.023
590 Yi, Y., Liska, M., Al-Tabbaa. 2013. A. Properties of two model soils stabilized with
591 different blends and contents of GGBS, MgO, lime, and PC. *Journal of Materials*
592 *in Civil Engineering*, 26, 267-274.
593 http://dx.doi.org/10.1061/(asce)mt.1943-5533.0000806